Compressive Sensing for No-Contact 3D Ground Penetrating Radar

Compressive Sensing for No-contact 3D Ground Penetrating Radar

Lapo Miccinesi, Neda Rojhani, and Massimiliano Pieraccini
Department of Information Engineering
University of Florence
Via Santa Marta, 3 50139 Firenze, Italy
massimiliano.pieraccini@unifi.it

***Abstract*—No-contact Ground Penetrating Radars (GPRs) are popular microwave sensors for investigating soils or masonry/stone walls. In this paper the authors evaluated the compressive sensing (CS) as possible technique for speeding up the acquisition time of this kind of application. In effect the CS approach could reduce the number of acquisition points, and then the measurement time by using only a random pattern of the antennas positions. The authors found that the data reconstruction loses quality even with a reduction of 25 % of the number of acquisitions, but the features of the targets still visible. With a reduction of 50 % the SNR decrease sensibly and most of the targets are not detectable. Such a time reduction results rather marginal in most practical cases.**

***Keywords*—compressing sensing (CS); ground penetrating radar (GPR); GPR imaging; no-contact GPR; orthogonal matching pursuit (OMP).**

I. INTRODUCTION

No-contact Ground Penetrating Radars (GPRs) are microwave sensors used for investigating soils or masonry/stone walls. Typical applications are: detecting buried mines [1] scanning walls to find possible damage [2] or hidden cavities [3],[4].

When the GPR operates with a single couple of antennas the measurement time can be very long, so its reduction could be desirable. There are two possible ways to do that: to reduce the integration time or to reduce the number of spatial steps. The first way is not viable because the high attenuation coefficient. On the other hand, to reduce the number of steps is forbidden by Nyquist theorem. Nevertheless, the compressive sensing (CS) theory offers a way to overcome the Nyquist limit and to reduce the number of spatial steps by using only a set of random positions of the antennas [5].

Generally speaking, CS is able to reconstruct a sparse signal by using a random set of samples of the signal [6], [7]. A signal of length N is sampled randomly M times, with M < N. Hence, in accord with the CS theory, the signal can be recovered by solving the convex optimization problem such as l_1-norm and basis pursuit [8]- [10].

However, the radar images reconstructed via CS lose quality, could be affected by artefacts and theirs signal-to-noise ratio (SNR) decrease [12].

II. THE RADAR EQUIPEMENT

The experimental data have been acquired using the radar equipment showed in Figure 1. The equipment was design as 3D painted walls scanner by two of the authors [4]. The scanner operates step-by-step both in frequencies and position. Two step motors move the radar head on a surface of 1.4 × 1.9 m² in a vertical plane. The radar operates a Step Frequency Continuous Wave (SFCW) with central frequency of 10 GHz and bandwidth of 4 GHz with 801 frequencies step (N_f). The output power in TX antenna was 19dBm. For each position of the antennas the device measured a complex number given by in-phase and quadrature components of the echo. The result of an entire acquisition is a three-dimensional matrix of complex numbers $N_f \times N_z \times N_x$ where N_z and N_x are respectively the number of positions of radar in z and x axis.

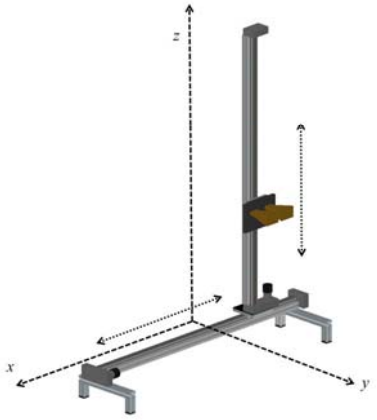

Figure 1. Sketch of the radar equipment

The integration time, $t_{int.}$, for all the measurement is given by (1).

$$t_{int} = N_x N_z N_f t_{tone} \quad (1)$$

Where t_{tone} = 10 ms, is the time of a single tone. By using N_x = 93, N_z = 126, N_f = 801 the integration time results to be t_{int} ≈ 26.1 hours. The integration time must be compared with the effective measurement time, t_{meas}, that include the movement

and data acquisition, that was 38.8 hours. Thus, the ratio t_{int}/t_{meas}, called duty cycle, has been 67.3 %.

III. The CS theory and focusing algorithm

For applying the CS theory, a pattern of N_A antennas has been selected randomly from each z coordinate of the echo matrix. For each frequency, the sampled vector, y, is define by [13]:

$$y = \Phi E \tag{2}$$

Where E is a sub-vector $N_x \times 1$ taken from the echo matrix and Φ is a binary random matrix, called measurement matrix, with size of $M \times N_x$ with $M > N_A$. For each row of the measurement matrix the non-zero elements are selected randomly from the allowed positions of the antennas pattern in the selected z-line.

The vector E is supposed to be represented on a $N_x \times N_x$ basis Ψ= fft(I), called dictionary, where fft(·) is the fast Fourier transform and I is the $N_x \times N_x$ identity matrix.

$$E = \Psi s \tag{3}$$

Where *s*, $N_x \times 1$, is the vector of weighting coefficients. By substituting (3) in (2), the sampled vector become:

$$y = \theta s \tag{4}$$

Where $\theta = \Phi\Psi$ is a $M \times N_x$ matrix. The vector E has to be reconstructed from the sampled vector, but retrieving a vector of length N_x from a set of M measurements (with $M < N_x$) is normally a ill-posed problem. This problem can be approached using the orthogonal matching pursuit (OMP) algorithm [10].

After reconstruction, the data have been focused by using a back-projection algorithm that considers the electromagnetic path between the antennas and any image point [14]. In order to evaluate the path between the antennas and image point, the Snell's law was applied. In other words, the length of the path has been evaluated by searching the minimum of travel time between two points in two different media: the antennas in air and the image point inside the wall [4].

IV. Simulation results

In order to test the CS algorithm a simulation has been implemented. A target has been placed inside a simulated wall of ε_2= 3.9 at a depth of 0.4 m. The distance between radar and wall was 1.6 m.

The image obtained (without CS) is shown in Figure 2. Figure 3 and Figure 4 show the results with a compression of 50 % and 30 %.

The SNR results to be $SNR_{100\%}$= 84.5 dB for image without CS, $SNR_{50\%}$= 29.0 dB for the image focused using 50 % of antennas' position and $SNR_{30\%}$= 26.5 dB using 30% of antennas' position.

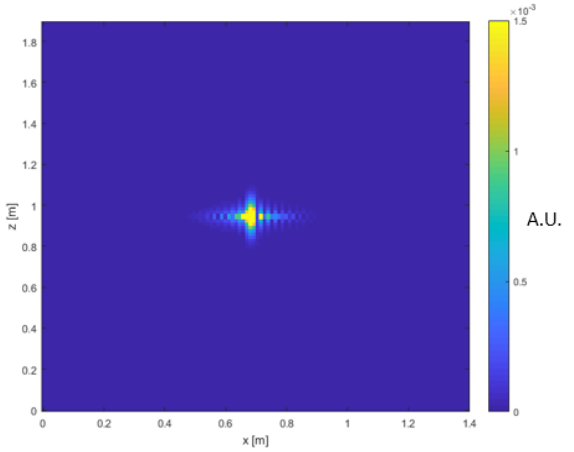

Figure 2. Power image of the simulated echo focused without CS

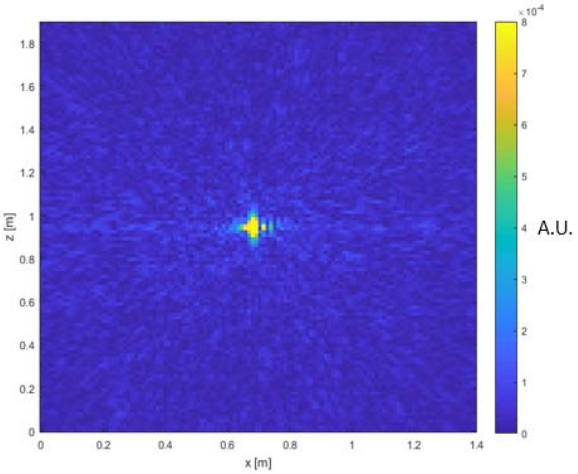

Figure 3. Power image of the simulated echo focused using 50 % of the antennas' positions

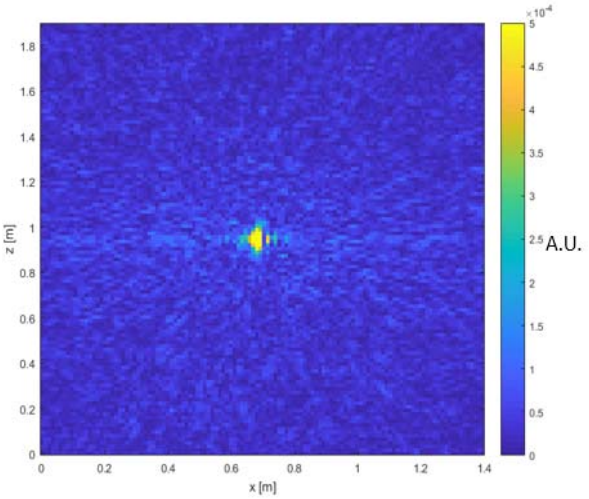

Figure 4. Power image of the simulated echo focused using 30 % of the antennas' positions

It results that in simulation, the reconstruction algorithm works successfully even with a reduction of 70 % (Figure 4)

of the antennas' positions.

V. Measurement Results

The CS algorithm was applied to a dataset acquired in a real scenario. The wall under test is shown in the background of Figure 5. The distance between the equipment and the wall was 1.6 m. The thickness of the wall is about 0.42 m. Two different depths inside the wall have been investigated.

The images have been focused without CS and with ratio N_A/N_x equal to 75 % and 50 %. For all images the SNR was found by considering the same target.

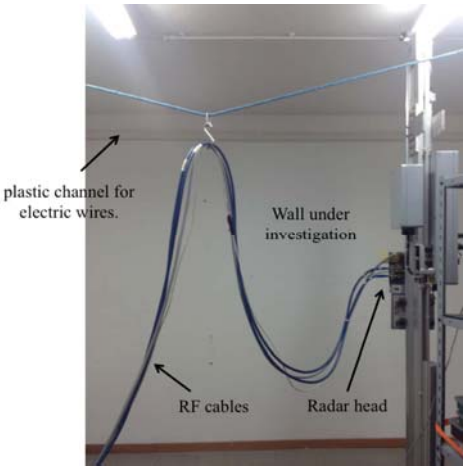

Figure 5. Picture of the wall under investigation

Figure 6 shows the focused image at 0.20 m inside the wall without CS. The red circles spotlight five different structures that are visible inside the wall. The SNR is evaluated for the target A at (x ≈ 0.4 m, z ≈ 1.2 m) and for target B at (x ≈ 0.2 m, z ≈ 0.2 m) and they result $SNR^A_{100\%}$= 21.8 dB, $SNR^B_{100\%}$= 20.8 dB.

As shown in Figure 7, with the percentage N_A/N_x of 75 % the signal-to-noise ratio decreases sensibly ($SNR^A_{75\%}$= 13.6 dB, $SNR^B_{75\%}$= 12.3 dB): only four of five targets are visible. With 50 % of the antennas' positions (Figure 8) only three targets of five are visible and SNR results to be $SNR^A_{50\%}$= 7.8 dB and $SNR^B_{50\%}$= 7.4 dB.

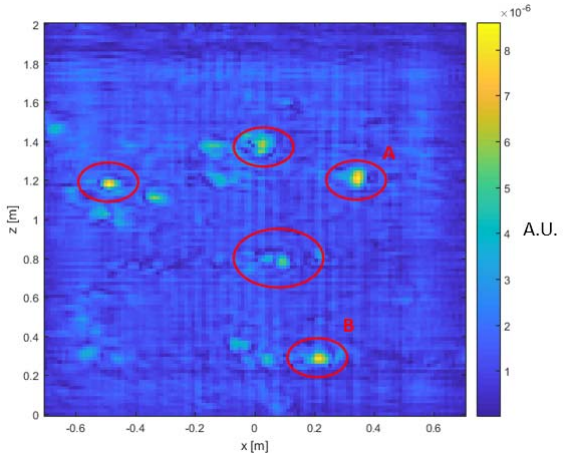

Figure 6. Power image focused on a vertical plane at 0.20 m inside the wall, without CS

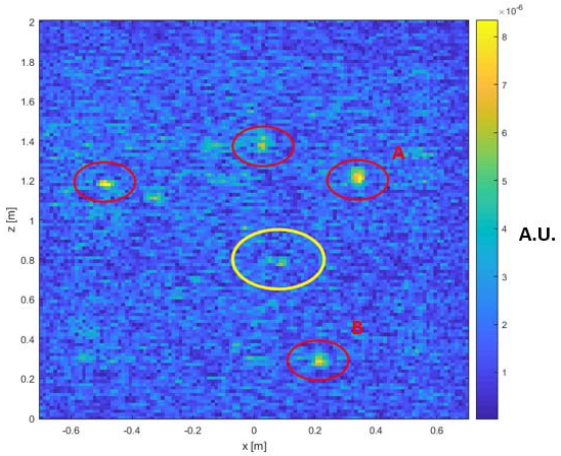

Figure 7. Power image focused on a vertical plane at 0.20 m inside the wall, with 75 % of the antennas' positions

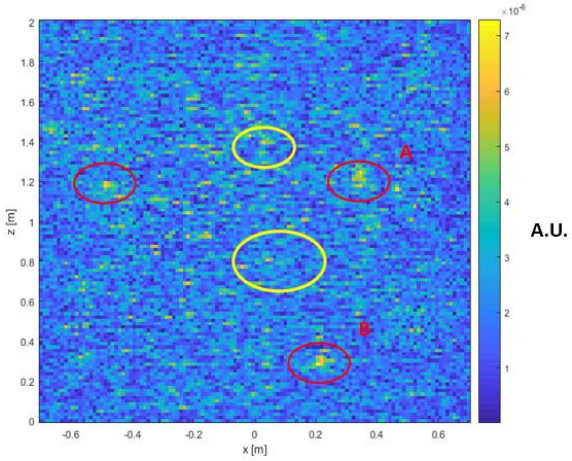

Figure 8. Power image focused on a vertical plane at 0.20 m inside the wall, with 50 % of the antennas' positions.

Figure 9 shows the image obtained by focusing at 0.40 m inside the wall without CS. In the picture there are seven well-visible targets. At z ≈ 0.3 m and z ≈ 1.3 m there are two electrical conduit pipes buried in the wall. The SNR was measured for the target located at (x ≈ 0.3, z ≈ 0.3 m). Without CS, SNR results to be $SNR_{100\%}$= 15.7 dB.

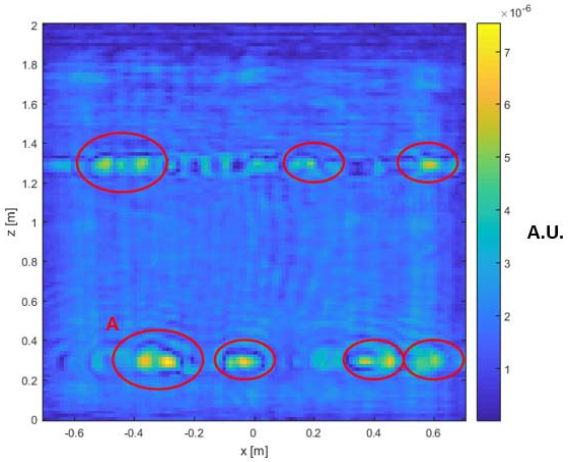

Figure 9. Power image focused on a vertical plane at 0.40 m inside the wall, without CS

The Figure 10 and Figure 11 show the image obtained with 75 % and 50 % of the antennas' positions. With N_A/N_x =75 % almost all the targets are visible, but it is not possible to recognize the shape of conduits at height of 1.3 m. The signal-to-noise ratio in this case is $SNR_{75\%}$ = 6.2 dB.

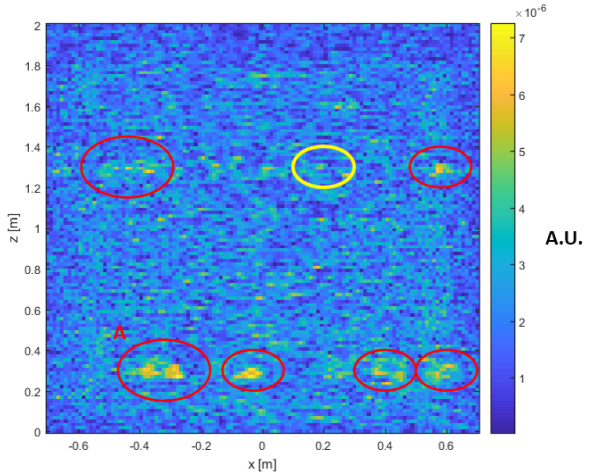

Figure 10. Power image focused on a vertical plane at 0.40 m inside the wall, with 75 % of the antennas' positions

With 50 % the targets are hardly visible and the shape of the electrical conduits is not recognizable. In this case the SNR is not well define.

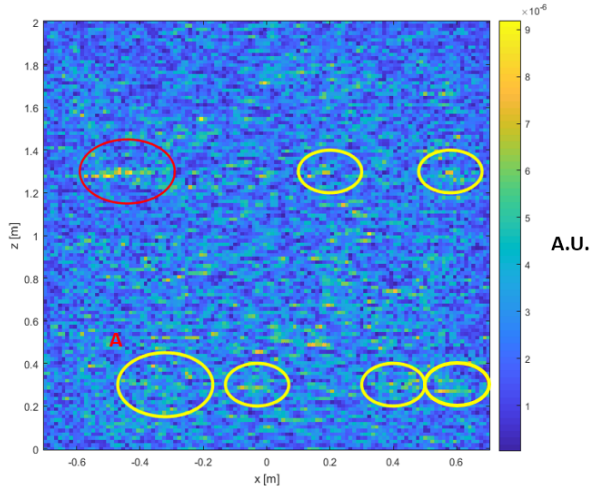

Figure 11. Power image focused on a vertical plane at 0.40 m inside the wall, with 50 % of the antennas' positions

VI. Conclusion

In this paper the CS technique is used to reduce the number of position of antennas to speed up a GPR scanner. The reconstruction algorithm was tested with a simulated dataset. The same reconstruction algorithm was used on dataset of a real scenario. Although the simulation shows that a reduction of 70 % of the antennas' positions could give images with well recognizable targets, the same algorithm used on an experimental data set gives image of low quality, even with a reduction of only 25 %. Probably the signal-to-noise ratio of GPR measurements is too low for sustaining the compressive sensing applied using the FFT of Kronecker delta as dictionary or to sustain OMP as retrieving algorithm. Nevertheless, other kinds of dictionaries or retrieving algorithm could be more effective. The author are searching to find a dictionary and a retrieving algorithm that can optimize the reconstruction for a GPR system.

References

[1] F. Lombardi, H. D. Griffiths, A. Balleri and M. Lualdi, "Preliminary results on multi offset GPR for imaging of landmines," *2017 9th International Workshop on Advanced Ground Penetrating Radar (IWAGPR)*, Edinburgh, 2017, pp. 1-6.

[2] H. Liu, C. N. Koyama, K. Takahashi and M. Sato, "High-resolution imaging of damaged wooden structures for building inspection by polarimetric radar," *Proceedings of the 15th International Conference on Ground Penetrating Radar*, Brussels, 2014, pp. 423-428.

[3] M. Pieraccini, D. Mecatti, G. Luzi, M. Seracini, G. Pinelli, C. Atzeni, "Non-contact intrawall penetrating radar for heritage survey: the search of the 'Battle of Anghiari' by Leonardo da Vinci." NDT & E International, Vol. 38, No. 2, pp. 151-157, March 2005

[4] M. Pieraccini, L. Miccinesi, *No-contact GPR for investigating painted walls,* 2018 17th International Conference on Ground Penetrating Radar (GPR), in press

[5] Chernyak, I. and M. Sato. *3D image reconstruction algorithm for a sparse array radar system based on compressive sensing*. in *Geoscience and Remote Sensing Symposium (IGARSS), 2017 IEEE International*. 2017

[6] Qaisar, S., et al., *Compressive sensing: From theory to applications, a survey.* Journal of Communications and networks, 2013. **15**(5): p. 443-456

[7] Jiang, J. and C. Chen. *Analysis in Theory and Technology Application of Compressive Sensing*. in *Intelligent Human-Machine Systems and Cybernetics (IHMSC), 2014 Sixth International Conference on*. 2014. IEEE

[8] Zhu, X.X. and R. Bamler, *Tomographic SAR inversion by $ L_ {1} $-norm regularization—The compressive sensing approach.* IEEE Transactions on Geoscience and Remote Sensing, 2010. **48**(10): p. 3839-3846.

[9] Cai, T.T. and L. Wang, *Orthogonal matching pursuit for sparse signal recovery with noise.* IEEE Transactions on Information theory, 2011. **57**(7): p. 4680-4688.

[10] Needell, D. and J.A. Tropp, *CoSaMP: Iterative signal recovery from incomplete and inaccurate samples.* Applied and computational harmonic analysis, 2009. **26**(3): p. 301-321.

[11] Zhang, L., et al., *Resolution enhancement for inversed synthetic aperture radar imaging under low SNR via improved compressive sensing.* IEEE Transactions on Geoscience and Remote Sensing, 2010. **48**(10): p. 3824-3838

[12] Qaisar, S., et al., *Compressive sensing: From theory to applications, a survey.* Journal of Communications and networks, 2013. **15**(5): p. 443-456.

[13] M. Pieraccini and L. Miccinesi, "ArcSAR: Theory, Simulations, and Experimental Verification," in *IEEE Transactions on Microwave Theory and Techniques*, vol. 65, no. 1, pp. 293-301, Jan. 2017